Research Square

Preprints are preliminary reports that have not undergone peer review.
They should not be considered conclusive, used to inform clinical practice,
or referenced by the media as validated information.

Fabrication and H2S gas sensitive performance of NiO ultrathin film encapsulated VO2(A) nanowire core-shell heterojunction structure

Jiran Liang

liang_jiran@tju.edu.cn

Tianjin University

Yingfu Zhang

Tianjin University

Xin Wen

Tianjin University

Kangqiang Wang

Tianjin University

Haigang Liu

Qinghai Chemical Design and Research Institute Co., Ltd

Qian He

Qinghai Chemical Design and Research Institute Co., Ltd

Xiaoping Gao

Gansu Academy of Sciences

Wenjun Yan

Hangzhou Dianzi University

Research Article

Keywords: VO2(A), NiO, Heterojunction, Chemical precipitation, Gas sensor

Posted Date: July 13th, 2026

DOI: https://doi.org/10.21203/rs.3.rs-10137674/v1

License: This work is licensed under a Creative Commons Attribution 4.0 International License.
Read Full License

Additional Declarations: No competing interests reported.

Fabrication and H_2S gas sensitive performance of NiO ultrathin film encapsulated VO_2(A) nanowire core-shell heterojunction structure

Jiran Liang[a,b,*], Yingfu Zhang[a], Xin Wen[a], Kangqiang Wang[a], Haigang Liu[c,d], Qian He[c,d], Xiaoping Gao[e], Wenjun Yan[f]

[a] School of Microelectronics, Tianjin University, Tianjin 300072, P.R. China.

[b] Tianjin Key Laboratory of Imaging and Sensing Microelectronic Technology, Tianjin University, Tianjin 300072, P.R. China.

[c] Qinghai Chemical Design and Research Institute Co., Ltd, Xining 810008, P. R. China.

[d] Qinghai Engineering and Technology Research Center of Fine Chemical, 810008, P. R. China.

[e] Key Laboratory of Sensor and Sensing Technology, Gansu Academy of Sciences, Lanzhou, Gansu 730000, P.R. China.

[f] School of Automation, Hangzhou Dianzi University, Hangzhou 310018, P.R. China.

[*] Corresponding Author E-mail Address: liang_jiran@tju.edu.cn (J. R. Liang)

Abstract:

High performance hydrogen sulfide (H_2S) gas sensor is highly desired to develop for the harmfulness of H_2S to human's health. In this work, a NiO/VO_2(A) nanowire core-shell heterojunction is constructed through chemical precipitation and annealing to improve the sensitivity to H_2S. The influence of precursor molar ratios on the composition, morphology, and gas-sensing performance of the core-shell heterojunction structure was investigated. The NiO/VO_2(A) nanowire core-shell heterojunction based sensor exhibits high sensitivity when the precursor molar ratio is 1:0.5. The gas response value is reached up to 11.57 to 1 ppm H_2S gas at 100 °C. And the gas sensor also shows excellent response and recovery characteristics. The high sensing performance is related to the heterojunction between VO_2(A) and ultrathin NiO film and the catalytic activity of NiO, which can enhance the chemical adsorption of oxygen on the surface of the heterojunction structure. The results suggest that VO_2(A) nanowires core-shell nanostructure have great potential for H_2S gas detection.

Keywords : VO_2(A); NiO; Heterojunction; Chemical precipitation; Gas sensor

1. Introduction

Hydrogen sulfide (H_2S) is a colorless gas with rotten egg smell. It can hurt the eyes, palsy central nervous system, and even cause die at high concentration. H_2S can composed explosive mixture with air, and lead to combustion and explosion when meets fire or at high temperature [1-3]. It is highly desired to develop a high performance gas sensor to detect H_2S for protecting human being from harming.

Metal oxide semiconductor material has been widely used in gas sensor as a functional material due to the advantages of sensing performance, low production cost and mature technology [4-6]. However, the high operation temperature of metal oxides semiconductor leads to an increase of power consumption and hardly integrate with integrated circuit.

A phase vanadium dioxide (VO_2(A)) nanowires exhibits obvious gas-sensitive response to H_2S gas at low temperature [7]. However, the sensitivity of pure VO_2(A) is relatively low and difficult to meet the demand for H_2S gas detection. The strategies of improving the sensitivity of gas-sensitive materials mainly include doping, precious metal modification, and heterojunction structure constructing [8-11]. Heterojunction is one of the strategy to improve the gas-sensitive performance for pure-phase metal oxide materials. But, it is still a challenge to select a suit oxide to construct the oxide heterojunction in improving the sensitivity of VO_2(A) material to H_2S. Nickel oxide (NiO) is a typical P-type metal oxide semiconductor material. It has low toxicity, high durability, and excellent catalysis [12-15], which shows great

potential in the enhancement H_2S detection of other metal oxide.

In this work, an ultrathin NiO film encapsulated VO_2(A) nanowire core-shell heterojunction structure is proposed to improve the H_2S sensing performance of VO_2(A). VO_2(A) nanowires were prepared by one step hydrothermal method. And the core-shell heterojunction structure was synthesized by chemical precipitation and high-temperature heat treatment method. The influences of NiO content on the sensing performance were investigated by varying the content of $Ni(NO_3)_2$ in the precursors in the chemical precipitation. The results showed that the gas-sensitive response of the sensor based VO_2(A)/NiO nanowire core-shell heterojunction structure synthesized at a precursor molar ratio of 1:0.5 to 1 ppm H_2S gas was up to 11.57 at 100 ºC, which was about 8 times higher than that of the pure phase VO_2(A) nanowires. It also shows good reproducibility and excellent H_2S gas selectivity. The enhancement of gas-sensitive performance of the composite structure can be attributed mainly to the synergy effects of catalytic and heterojunctions effect.

2. Experimentals

2.1 Synthesis of VO_2(A) nanowires

VO_2(A) nanowires were prepared by one step hydrothermal method. Vanadium pentoxide powder is the vanadium source and the weight is 0.56 g. Oxalic acid dihydrate is the reductant and the weight is 0.58g. These two raw materials were added to 70 ml deionized water. And then, the solution was rapidly stirred for 60 min to form an uniformly disperse mixed solution. The mixed solution was annealed at 220 °C and kept for 36 h in 100 ml Teflon-lined autoclave. The VO_2(A) nanowires

powder was obtained by washing the resulting precipitates and drying at 60 ℃ for 12 h.

2.2 Synthesis of VO_2(A)/NiO nanowire core-shell heterojunction structure

VO_2(A)/NiO nanowire core-shell heterojunction structures were prepared by the chemical deposition on VO_2(A) nanowires and annealing. The preparation process is shown in Fig. 1. Firstly, $Ni(NO_3)_2$-$6H_2O$ was dissolved in 45 mL deionized water to obtain $Ni(NO_3)_2$ solution, and then 0.1 g of VO_2(A) nanowires powder was added to the solution. The mixture solution was stirred magnetically until all the additive was dissolved.

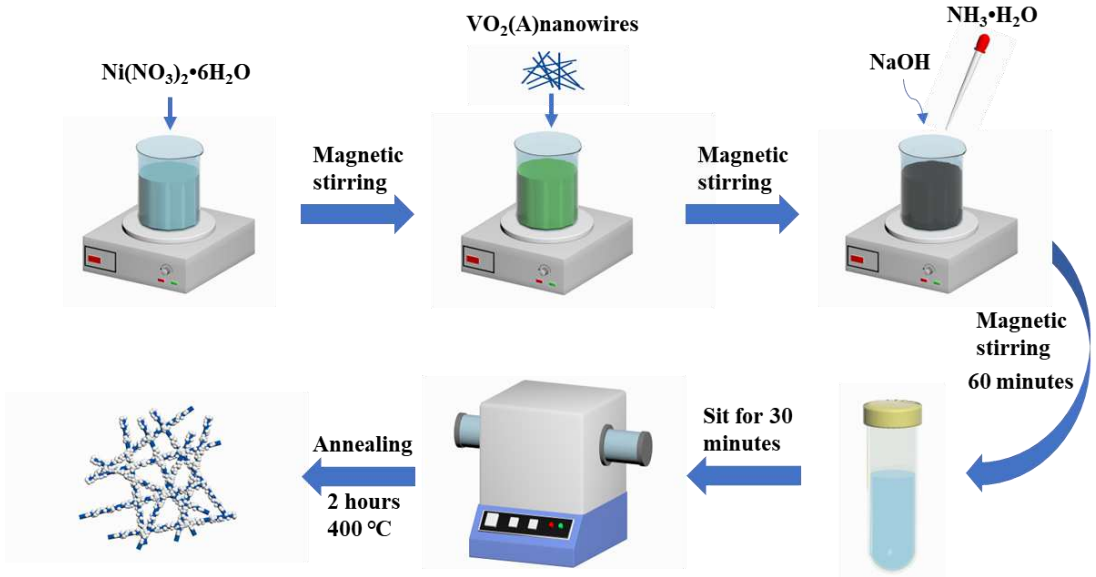


Fig. 1 Flow chart of VO_2(A)/NiO nanocomposite structure preparation

1.5 mL of ammonia (13.38 mol/L) and 0.1 g of NaOH were added to the resulting solution in turn. Magnetic stirring for 15 min was carried out to completely dissolve the NaOH in the solution. The solution was placed at room temperature for

30 min, until a layering of the solution was observed with sediment on the bottom of the beaker. The solution was placed in a centrifuge tube and washed several times with deionized water and anhydrous ethanol alternately. Then the samples were dried in an oven at 60 ℃ for 12 h. After drying, the samples were placed in a tube furnace and annealed in an argon atmosphere for 2 h at 400 °C. The heating rate was 5 °C/min. $Ni(OH)_2$ is decomposed at high temperatures and changes to NiO. The VO_2(A)/NiO nanowires core-shell hetrojunction structures were obtained. The NiO content in VO_2(A)/NiO nanocomposite structures is a key parameter affecting the sensing performance. In order to investigate the influence of NiO content on the sensing performance, a set of samples with different NiO content were prepared by changing the content of $Ni(NO_3)_2$ in the precursors. The samples with V and Ni molar ratios of 1:0.5, 1:1, and 1:2 were labeled as R-0.5, R-1, and R-2, respectively.

2.3 Characterization

The composition of the obtained samples was analyzed by X-ray diffractometer (XRD, MiniFlex600) with Cu Kα radiation (λ=1.54059 Å). The morphological structure of the samples was measured by thermal field emission scanning electron microscopy (FESEM, JSM-7800F). The elemental composition and distribution of the samples were measured by the energy dispersive spectrometer (EDS) equipped with the FESEM system. To further investigate the influence of precursor molar ratio on the microstructure, the VO_2(A)/NiO nanowires core-shell hetrojunction structure microscopic morphology was characterized by transmission electron microscopy (TEM, JEM-2100F).

2.4 Gas sensor fabrication and gas sensing characterization

The VO_2(A)/NiO based sensor was fabricated through coating VO_2(A)/NiO ultrasonically dispersed suspension on the surface of the gold interdigital electrode. After coating, the sensor was dried at 60 °C for 30 min.

In order to characterize the gas sensing performance, the dynamic response of the fabricated sensor to different gas were carried out by a manmade gas sensing measurement system. The sensing measurement system has four parts: chamber, temperature control device, data acquisition system, and a small fan. The resistance of the gas sensor with or without was measured by a high-precision digital multi-meter (NUI-T UT70D). The target gas was introduced into the chamber with a micro-injector, and the volume can be tuned by micro-injector. The gas concentration can be obtained by calculating the volume ratio of the injected gas to the chamber. The resistance of the sensor with gas concentration was recorded dynamically by the data acquisition system. The gas response (S) of the sensor is calculated according to $S = R_g / R_a$, where R_g and R_a is the resistance of the gas sensor in the target gas and in air at the stable state, respectively. The response and recovery time were obtained from the dynamic response curve, which defines as the time taken for the resistance change of the gas sensor to the 90% of the total resistance change during the injection and removal process.

2.5 Density functional theory (DFT) calculation method

The adsorption effect of H_2S molecule on the surface of VO_2(A)/NiO heterojunction structure was investigated through the first-principles calculations

based on density functional theory. CASTEP module was used to perform the calculations in Materials Studio software. The GGA-PBE method was used to characterize the exchange and correlation energies. And the cutoff energy for the plane-wave expansion is set to 660 eV. The K-points of the Monkhorst-Pack lattice sampled from the Brillouin zone was 1×1×1. In order to prevent the interactions between the periodic structures, a 10 Å vacuum layer was coated on the surface of NiO. In order to optimize the geometry, the convergence tolerance was set to 1.0×10^{-4} eV/atom for energy, 0.03 eV/Å for maximum force, 0.05 GPa for maximum stress, and 1.0×10^{-3} Å for maximum displacement.

3. Results and Discussion

3.1 Morphology and structural characterization of VO_2(A)/NiO structures

The XRD diffraction patterns of the synthesized VO_2(A)/NiO structures are shown in Fig. 2. There are obvious diffraction peaks in the XRD diffraction patterns of the three samples, as shown in Fig. 2a. The diffraction peaks at 2θ = 14.86°, 29.94° and 45.6°, corresponds to (110), (220,) and (330) crystal planes of the tetragonal phase VO_2(A) according to diffraction card JCPDS:42-0876, respectively [16]. The diffraction peaks at 2θ = 37.22°, 43.24°, and 62.96° corresponds to (110), (-111), and (111) crystal planes of NiO (JCPDS:89-7131), respectively [17]. The XRD results suggest that both NiO and VO_2(A) components are contained in the nanocomposite structure obtained at different NiO content. In order to investigate the effect of NiO content on the composition of composite structure, diffraction peaks in the XRD patterns with 2θ values in the range of 35° to 50° were magnified, and the

corresponding local patterns are shown in Fig. 2 (b). It can be seen from the figure that the diffraction peaks belonging to NiO in the R-0.5 sample are relatively weak, and the intensity of NiO diffraction peaks increases gradually with the molar ratios increase of $Ni(NO_3)_2$ in the precursors.

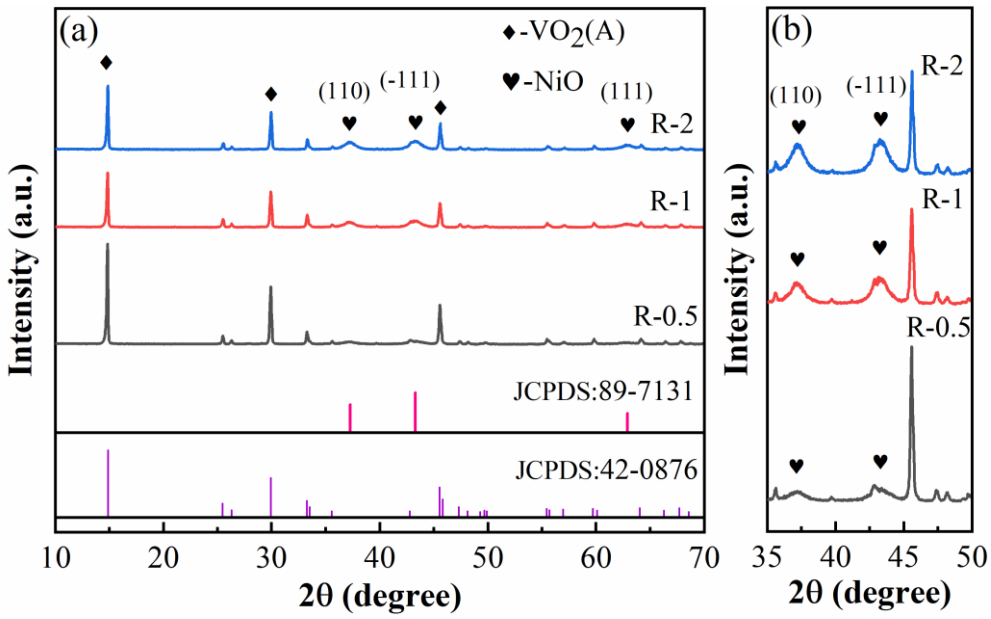


Fig. 2 (a) XRD patterns of samples with different molar ratios, (b) local magnification

The surface morphology of the samples with precursor molar ratios of 1:0.5, 1:1, and 1:2 were characterized by SEM, as shown in Figure 3. Figure 3 a, c, e is the original image, and Figure 3 b, d, f is the magnified view correspondingly. From Figure 3, it can be seen that the VO_2(A) nanowires are randomly staggered on the surface of substrate, which is convenient for gas diffusion. The cross-section of VO_2(A) nanowires is rectangular structure [7], and was not melted or deformed at the high temperature annealing.

Figure 3 (a) shows the morphology of the R-0.5 sample. Compared with the pure VO_2(A) nanowires, there are many small irregular nanoparticles attached to the smooth surface of the VO_2(A) nanowires, making the surface of the nanowires rough. This rough surface indicates that NiO was successfully coated on the surface of the nanowires, and the VO_2(A) nanowires and NiO with a thin sheet-like structure were cross-stacked together in the composite sample.

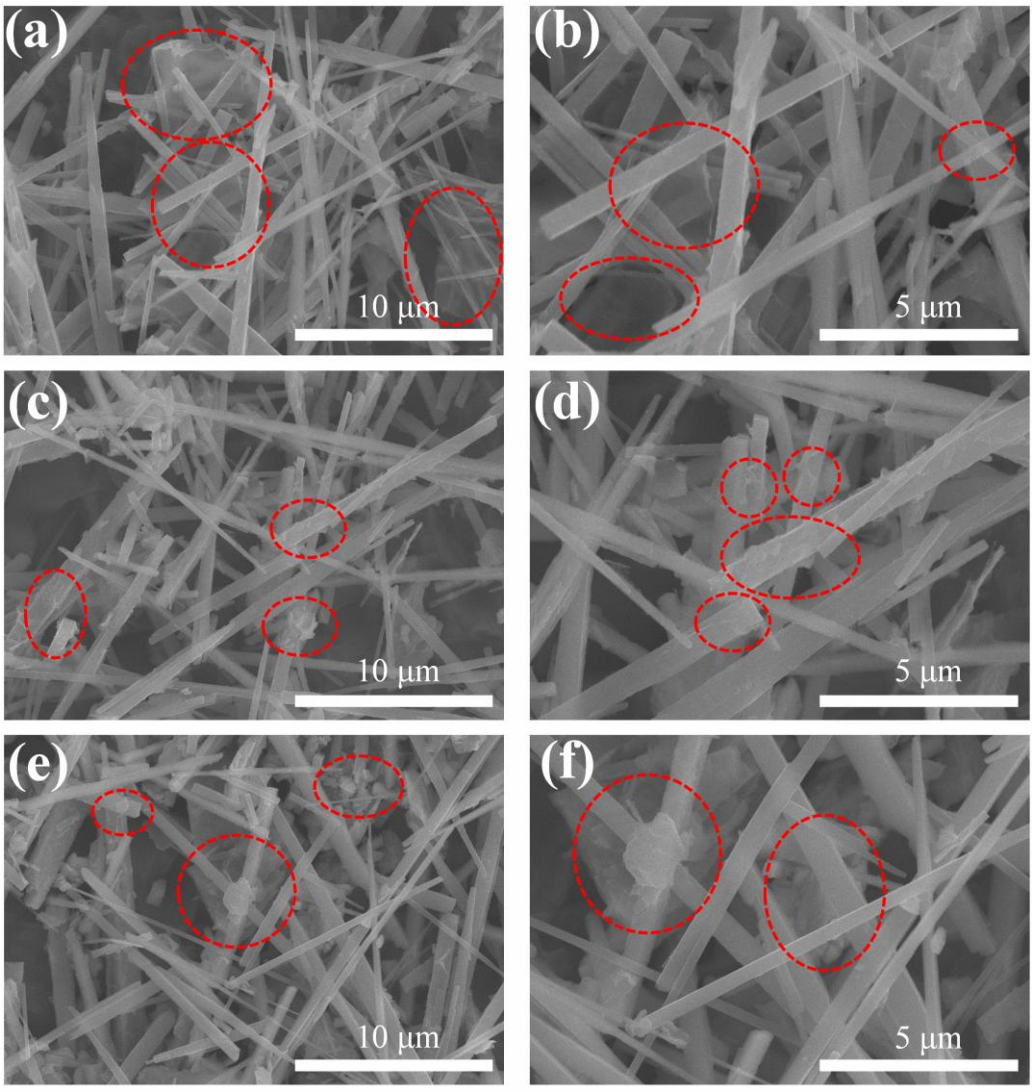


Fig. 3 SEM images of samples at different molar ratio, (a) and (b) SEM images of different magnifications of R-0.5, (c) and (d) SEM images of different magnifications of R-1, (e) and (f) SEM images of different magnifications of R-2

It is more clear from the high amplification SEM image, Figure 3 (b), the nanosheet is ultrathin, making it transparent. Figures 3 (c) and (d) show the SEM images of the R-1 sample. With the increase of $Ni(NO_3)_2$ ratio in the precursors, the NiO gradually changes it shape from nanosheets to a particle-like structure. For the R-2 sample, due to the excessive amount of $Ni(NO_3)_2$ in the preparation process, NiO not only grows on the surface of the VO_2(A) nanowires but also tends to gather and generate large bulk structures, as shown in Figures 3 (e) and (f).

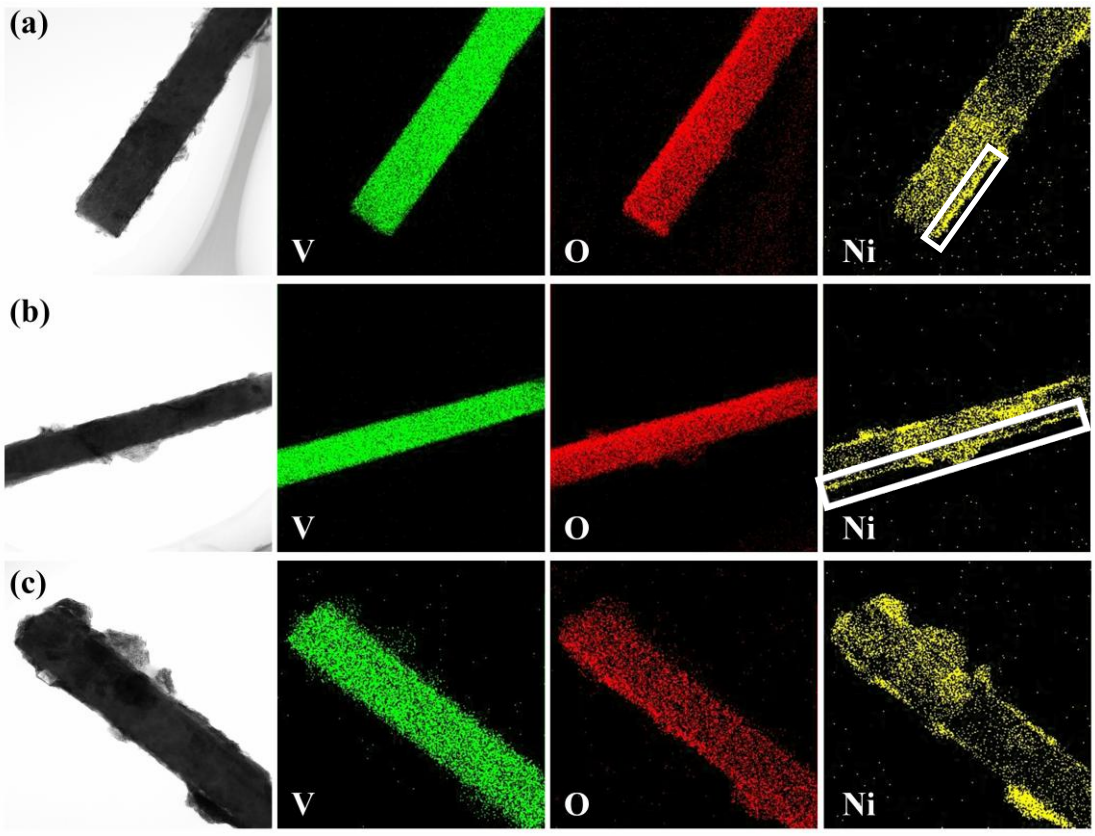


Fig. 4 (a) Elemental distribution of single nanowires in R-0.5 sample, (b) elemental distribution of single nanowires in R-1 sample, (c) elemental distribution of single nanowires in R-2 sample

In order to characterize the distribution of the composition in the composite structure surface, EDS measurement were carried out for the three samples. Figure 4 shows the elemental distribution on single nanowires surface of the samples, in which the green color represents the V elements, while the red and yellow colors represent the O and Ni elements, respectively. It can be seen that three elements, V, O, and Ni, are distributed on the nanowires after the synthesis. In particular, two elements, V and O, show a uniform distribution on the nanowire.

From the Ni element distribution image, it can be found that Ni element distributes on the surface of VO_2(A), but it is not uniform. The Ni on the surface is continuous and dense in sample R-0.5, which suggests that NiO is a continuous thin film on the VO_2 nanowire surface (as shown in Figure 4a). And there are also some nanoparticles on the surface. As the content increasing, the size of NiO nanoparticles increases, but the thickness of the NiO film decreases in sample R-1, as shown in the white rectangle of Figure 4b. When the content increased further, the number and size of NiO nanoparticles increase obviously. But, the thickness of NiO thin film on the nanowires surface changes not obvious, as shown in Figure 4c. This variation of thickness may be related to the NiO nanoparticles. With the content increasing, NiO is grown on the nanoparticles, not on the film. This further indicates that NiO has been successfully encapsulated on the surface of VO_2 (A) nanowires by a combination of chemical precipitation and high-temperature heat treatment.

To further characterize the microstructure of nanocomposite core-shell structures, TEM measurement was carried out. Figure 5 shows the TEM images of the

samples with different molar ratios. From these figures, it can be found that after chemical precipitation and high-temperature heat treatment, the originally smooth surface of the samples became rough, and an irregular layer of nanoparticles was wrapped on the surface of the nanowires, thus forming a core-shell structure with VO_2(A) nanowires as the core. And with the increase of precursor molar ratio during chemical precipitation, the number and size of nanoparticles on the nanowire surface gradually increases.

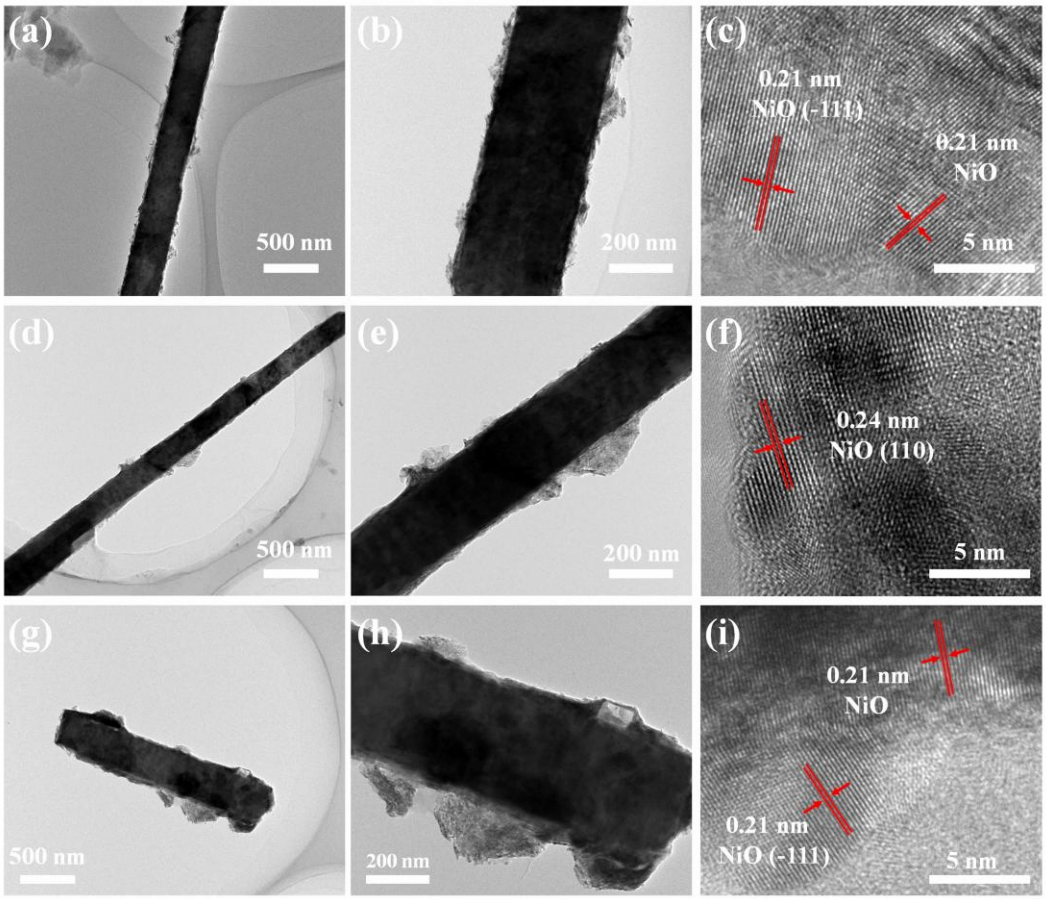


Fig. 5 TEM images of samples with different molar ratios, (a)-(b) TEM images of R-0.5 samples, (c) HRTEM images of R-0.5 samples; (d)-(e) TEM images of R-1 samples, (f) HRTEM images of R-1 samples; (g)-(h) TEM images of R-2 samples, (i) HRTEM images of R-2 samples

Next, in order to confirm the components and lattice structure of the nanowire surface shell layer, HRTEM characterization was conducted. Figures 5 (c), (f), and (i) show the HRTEM images of the R-0.5, R-1, and R-2 samples, respectively, which clearly show the lattice stripes of the shell layer that wrapped around the surface of the nanowires. The inter-planar spacing between the two lattice stripes in the R-0.5 and R-2 samples is 0.21 nm, which corresponds to the (-111) crystal plane of NiO. The distance between two lattice stripes in the R-1 sample is 0.24 nm, which corresponds to the (110) crystallographic plane of NiO. This further indicates that the nanoparticles uniformly coated on the nanowire surface are NiO, which is consistent with the previous EDS test results.

3.2 Gas-sensitive performance of VO_2(A)/NiO nanocomposite structures

The gas-sensitive responses performance of the sensors based on the synthesized nanowires core-shell hetrojunction structure was firstly tested for 1 ppm H_2S at different operation temperature. The relative humidity is 25% at 25 ℃. The test results are shown in Figure 6. It can be observed that the response of the R-0.5 and R-1 samples gradually decreased with the increase of operation temperature. The response value of the R-0.5 sample to 1 ppm H_2S decreased from 16.4 at 25 ℃ to 4.47 at 200 ℃, while the response value of the R-1 sample decreased from 8.79 to 1.86. For the R-2 sample, however, its gas-sensitive response to 1 ppm H_2S showed an increasing trend with the operation temperature, and reached the maximum value at 150 ℃. The increase of the R-2 sample with the working temperature is mainly related to the higher content of NiO in the composite structure. NiO generally needs to work at a higher temperature to obtain enough energy to achieve the transfer of

electrons and the adsorption and desorption of gas molecules [18]. So, the working temperature for R-0.5 and R-1 is room temperature, while 150 ℃ for R-2.

In addition, by comparing the response curves of the samples, it can be found that the R-0.5 sample to 1 ppm H_2S is significantly higher than that of the other samples when the operating temperature is below 150 °C. Although the sensitivity of the R-2 sample reached the maximum value of 10.24, it was still lower than that of the R-0.5 sample at 150 °C. The composite sample prepared at the precursor molar ratio of 1:0.5 has high sensitivity, low operating temperature, and the best corresponding gas-sensitive performance, so the next gas-sensitive test is mainly focused on the R-0.5 sample.

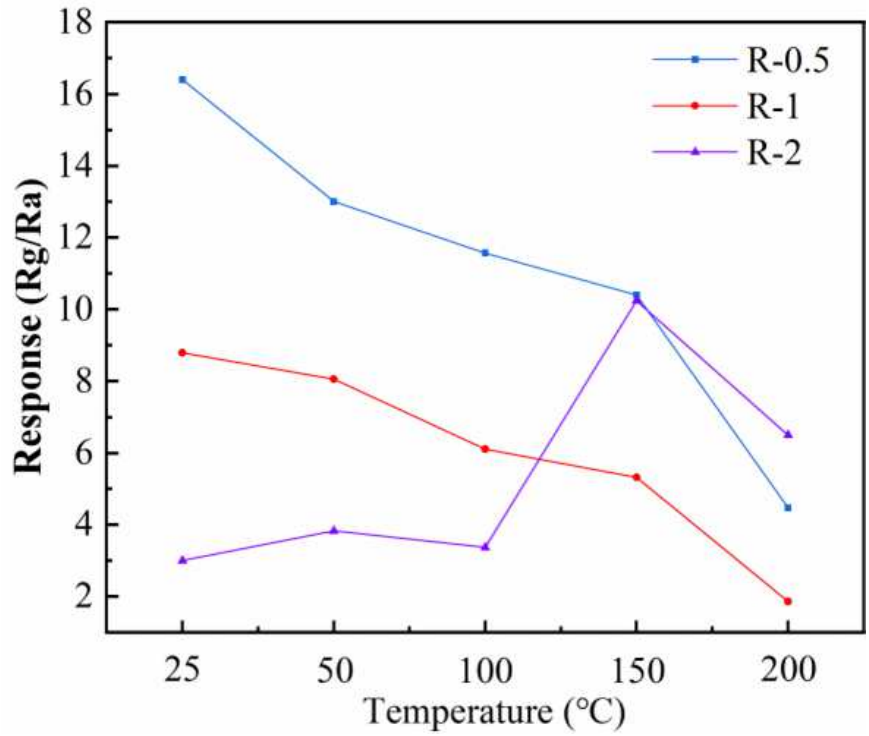


Figure 6 Gas-sensitive response of R-0.5, R-1 and R-2 samples to 1 ppm H2S at different operating temperatures

Figures 7 (a)-(e) show the single dynamic response curves of sample R-0.5 to 1 ppm H_2S at different operating temperatures. When the target gas is introduced, the resistance value of the sensor increases sharply, which suggests that R-0.5 sample shows the gas-sensitive characteristics of a p-type semiconductor exposed to H_2S gas [19]. The response to 1 ppm H_2S gas reaches 16.4 at room temperature, which is 11.9 times higher than that of the pure phase VO_2(A) nanowire (the pure VO_2(A) to H_2S is 1.38) [7]. However, the disadvantage is that the sensor resistance does not recover normally after the gas is exhausted. And with the increase of the operating temperature, the gas response value decreased, but shows a better recovery performance. And the higher the operating temperature, the shorter the recovery time. When the working temperature is 100 ℃, the gas response of the R-0.5 sample to 1 ppm H_2S gas can still reach 11.57 and has good response/recovery characteristics. As shown in Fig. 7 (f), the recovery time of the gas-sensitive sensor based on the R-0.5 sample is 257 s at this operating temperature. Therefore, from the perspective of the practical application of the sensor, 100 °C is chosen as the working temperature for the sensor in the next gas-sensitive test.

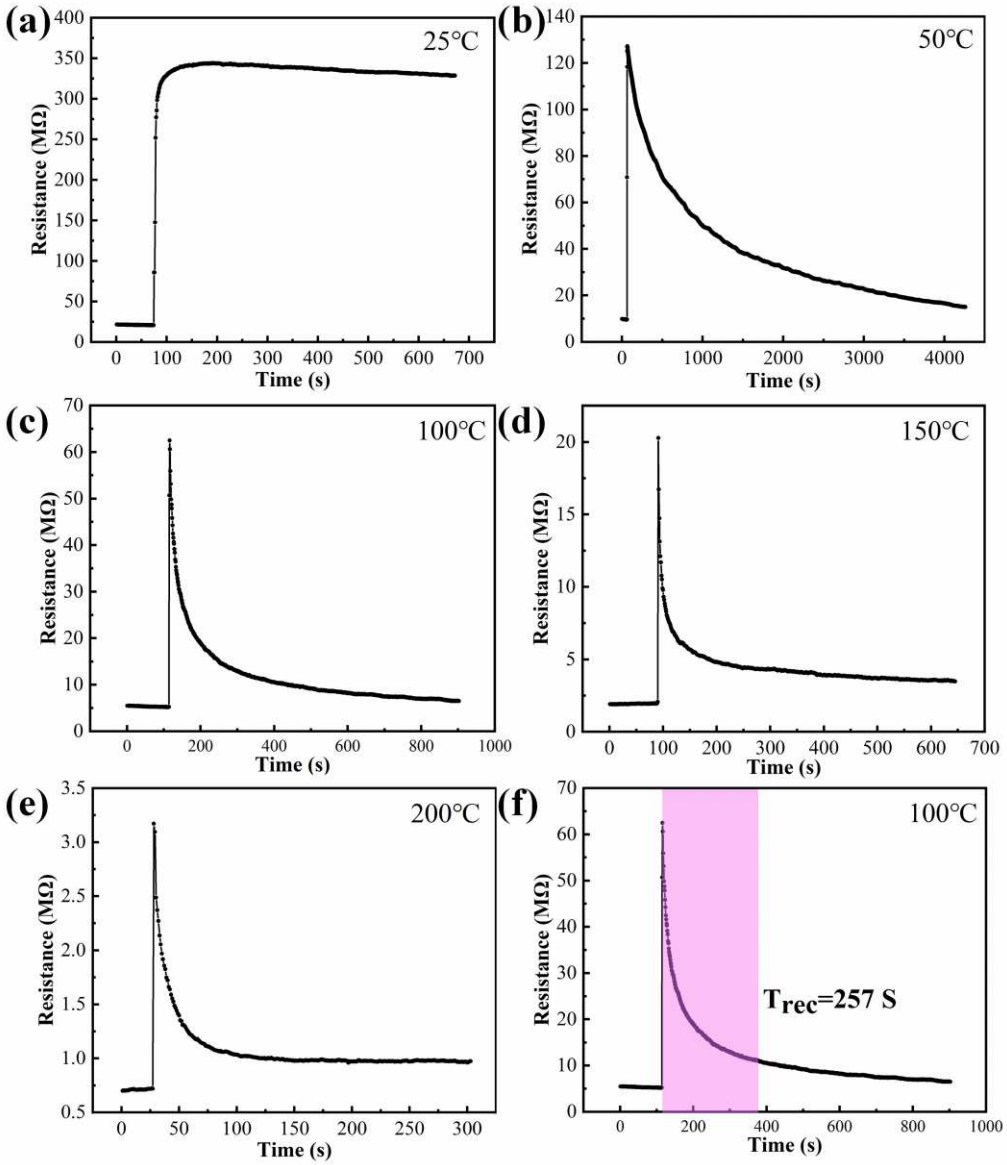


Figure 7 Dynamic response curves of R-0.5 samples to 1 ppm H_2S at different operating temperatures (a) 25 °C, (b) 50 °C, (c) 100 °C, (d) 150 °C, (e) 200 °C, (f) recovery time of R-0.5 samples to 1 ppm H_2S gas at an operating temperature of 100 °C

Repeatability is also an important index for evaluating the gas-sensitive performance, and the better repeatability of a sample during target gas detection indicates higher reliability and stability. To measure the repeatability of the R-0.5 sample, its gas-sensitive response to 1 ppm H_2S gas was continuously tested at an

operating temperature of 100 °C. Figure 8 shows the repeatability curve of the R-0.5 sample, which shows that the R-0.5 sample showed similar recovery characteristics without any significant decrease in sensitivity, indicating that the R-0.5 samples have good reproducibility.

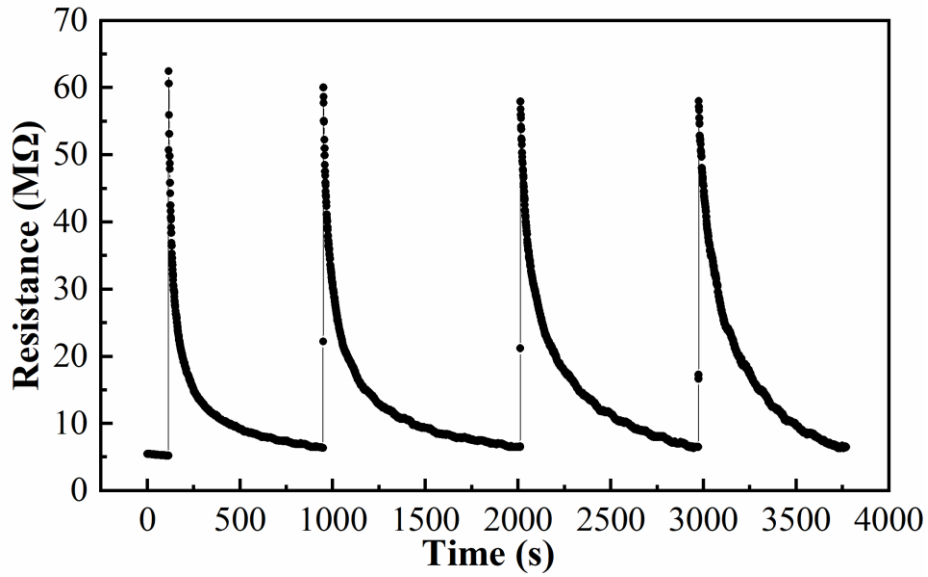


Figure 8 Repeatability response curve of R-0.5 sample to 1 ppm H_2S at an operating temperature of 100 °C

For the application of gas sensors, selectivity is also a vital factor to be considered. We selected methanol, ethanol, acetone, and toluene as the interfering gases, and measured the gas-sensitive response of the R-0.5 sample to these four gases at an operating temperature of 100 ℃. The results are shown in Figure 9. The response of sample R-0.5 to 50 ppm methanol, ethanol, acetone, and toluene was 1.14, 1.17, 1.08, and 1.1, respectively. All the response value was much lower than that of R-0.5 to 1 ppm H_2S, which indicates that the R-0.5 sample shows excellent selectivity to H_2S gas.

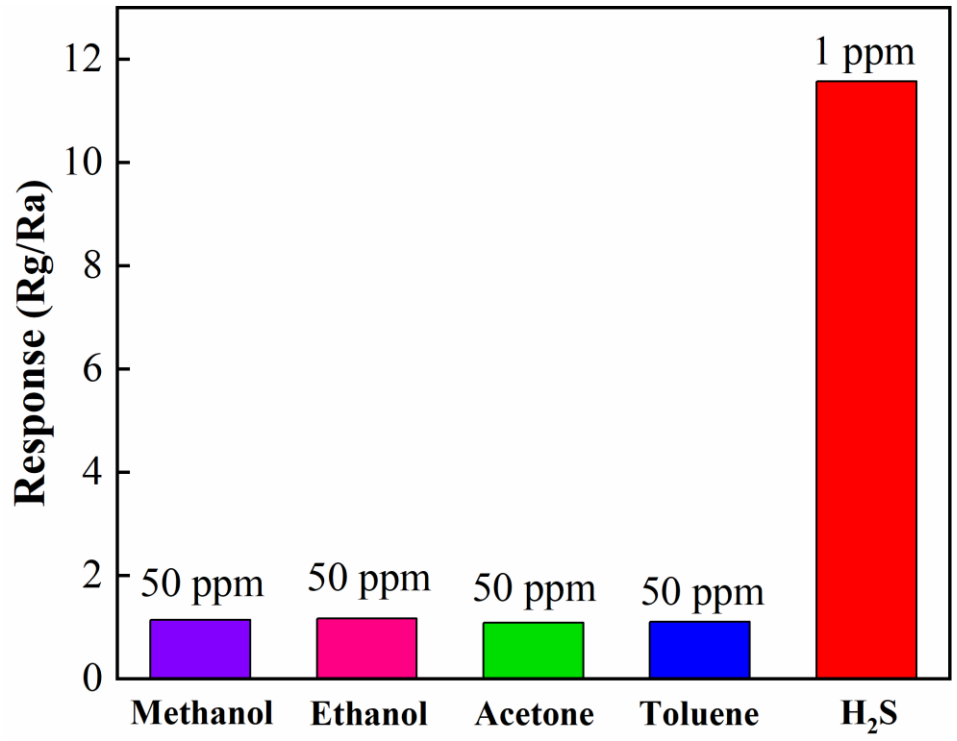


Figure 9 Gas-sensitive response of R-0.5 samples to different gases

Table 1 shows the comparison of the gas-sensitive performance of VO_2(A)/NiO nanocomposites with other H_2S-sensitive materials. It can be seen that the VO_2(A)/NiO nanocomposite has greater advantages in H_2S gas detection. Compared with the pure phase VO_2(A) nanowires, the response was greatly improved. The operating temperature is also lower compared to other composites or single structure, which will significantly reduce the power consumption of gas sensors and is also more helpful for their practical applications. Therefore, VO_2(A)/NiO nanocomposites are expected to be suitable candidates for the fabrication of high-performance H_2S gas-sensitive sensors.

Table 1 Comparison of gas-sensitive performance

Sensitive material	Structure	Target gas	Concentration	response	Operating temperature	Ref.
VO_2(A)	nanowire	H_2S	10 ppm	2.09	Room temperature	Ref.[7]
NiO	nanoparticle film	H_2S	100 ppm	9.71	250℃	Ref.[20]
NiO	porous microspheres	H_2S	20 ppm	27.2	200 ℃	Ref.[21]
V_2O_3/NiO	nanoflower	H_2S	0.5 ppm	6.5	200 ℃	Ref.[22]
CuO/NiO	core-shell microspheres	H_2S	100 ppm	47.6	260 ℃	Ref.[23]
VO_2(A)/NiO	core-shell nanowires	H_2S	1 ppm	11.57	100 ℃	This work

3.3 Density Functional Theory (DFT) Investigation

In order to clarify the sensing enhancement reason of core-shell heterojunction structure, a VO_2(A)/NiO heterostructure model was established to simulate the gas adsorption configurations by DFT. The gas adsorption configuration is shown in Figure 10 (a). The DFT simulations select the VO_2(A) (110) plane and the NiO (-111) plane to construct the heterostructure. The adsorption energy was calculated as:

$$E_{ads}=E_{system+gas}-E_{system}-E_{gas} \quad (1)$$

where E_{ads} is the calculated adsorption energy, $E_{system+gas}$ is the energy of the VO_2(A) and NiO systems with the adsorbed gas, and E_{system} and E_{gas} are the energies of the VO_2(A) and NiO systems and a single H_2S molecule, respectively. The positive adsorption energy indicates an endothermic adsorption process, which is unfavorable for gas adsorption and sensing. Conversely, a negative adsorption energy indicates an exothermic adsorption process, suggesting spontaneous adsorption.[24-25].

According to those calculations, we identified the stable adsorption configuration of H_2S molecules on the heterostructure of VO_2(A) and NiO. The adsorption energy

of H_2S molecules on the surface of VO_2(A)/NiO heterostructure was -39.01 eV. This result indicates that the adsorption process is exothermic and could occur spontaneously.

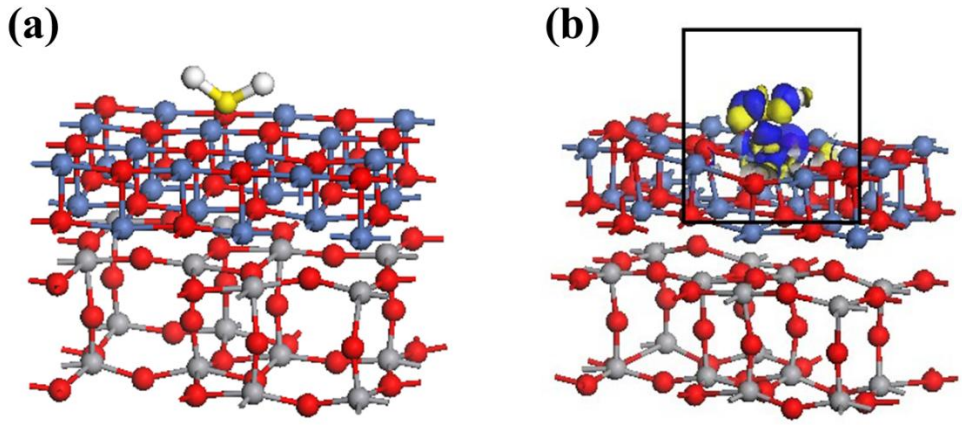


Figure 10 (a) Gas adsorption configurations of vanadium dioxide and nickel oxide forming heterojunctions, (b) Charge density difference for H_2S adsorbed on VO_2(A)/NiO heterostructure.

Charge Density Difference (CDD) can be used to analyze the charge transfer in the heterojunction structure interacted with gas adsorption. Gas adsorption configurations of VO_2 and NiO was shown in Figure 10 (b), red atom is oxygen atom, gray atom is vanadium atom, and blue atom is nickel atom. The yellow area represents a decrease in electron density, while the blue area represents an increase in electron density.

It can be seen from Figure 10 (b) H_2S molecule is surrounded by the yellow area, and a blue area is occurred between the gas molecule and the NiO surface. This phenomenon indicates that H_2S transfers electrons to the VO_2(A)/NiO nanocomposite

structure during the interaction between H_2S molecules and NiO. This result further confirms that the adsorption process of H_2S could occur spontaneously.

3.4 Gas-sensitive mechanism of VO_2(A)/NiO nanocomposite structures

The H_2S gas-sensitive response is improved greatly by additive NiO ultrathin nanothin film compared to that of the original one-dimensional VO_2(A) nanowires. The enhancement of the gas-sensitive performance by the core-shell hetrojunction structure can be attributed mainly to the following two factors.

(1) catalytic effect of NiO ultrathin film

The sensing response of metal oxide semiconductors to H_2S gas depend essentially on the chemisorbed oxygen on their surfaces and the reaction between the H_2S molecules and the formed oxygen ions. The corresponding reaction process at room temperature is shown as follows.

$$O_2(gas) \rightarrow O_2(ads) \quad (2)$$

$$O_2(ads)+e^- \rightarrow O_2^-(ads) \quad (3)$$

$$2H_2S(gas)+3O_2^-(ads) \rightarrow 2H_2O(gas)+2SO_2(gas)+ 3e^- \quad (4)$$

From the SEM and TEM characterization results of VO_2(A)/NiO nanocomposite structure, we can find that NiO ultrathin film is distributed on the surface of VO_2(A) nanowires and forms a core-shell structure. There is a part of NiO ultrathin nanosheet and particle-like structure on the nanowires. It is known that NiO shows high catalytic activity and can enhance the chemisorption of oxygen on the surface of the nanocomposite structure [26]. This high catalytic activity promotes the formation of oxygen ions and increases the number of oxygen ions in a certain degree. When the

reducing gas H_2S reacts with the oxygen ions, electrons will be released to the nanocomposite structure, which causes a change of the resistance. In addition, the composited NiO on the surface of the nanowires also has a catalytic effect for the oxidation of H_2S [27], which is conducive to promoting the reaction, leading to an increase in the gas-sensitive response of the VO_2(A)/NiO nanocomposite structure. Thus, the catalytic effect of NiO plays an important role in enhancing the gas sensing performance of the nanocomposite structures.

(2) Heterojunction effect

P-type NiO nanoparticles were integrated with n-type VO_2(A) nanowire by annealing. A N-P heterojunction was formed at the interface of the two oxides. Free electrons migrate from VO_2(A) to NiO due to the lower work functions of VO_2(A) [28-29]. The holes move in the opposite direction to VO_2(A) until the Fermi energy levels (E_F) of the two materials reach a balanced state, as shown in Figure 11 (a). At this time, a hole depletion layer is formed on the NiO side, and an electron depletion layer is formed at the VO_2(A) side, and then an inversion layer is formed on the surface of VO_2(A) due to the excessive bending of the energy band at the interface, which makes the forbidden band midline Ei higher than the E_F of VO_2(A). At the time, a potential barrier is also created at the bending interface of the energy band, resulting in a significant increase in the resistance of the VO_2(A)/NiO nanocomposite structure, which is considerably greater than that of the main material, VO_2(A) nanowires.

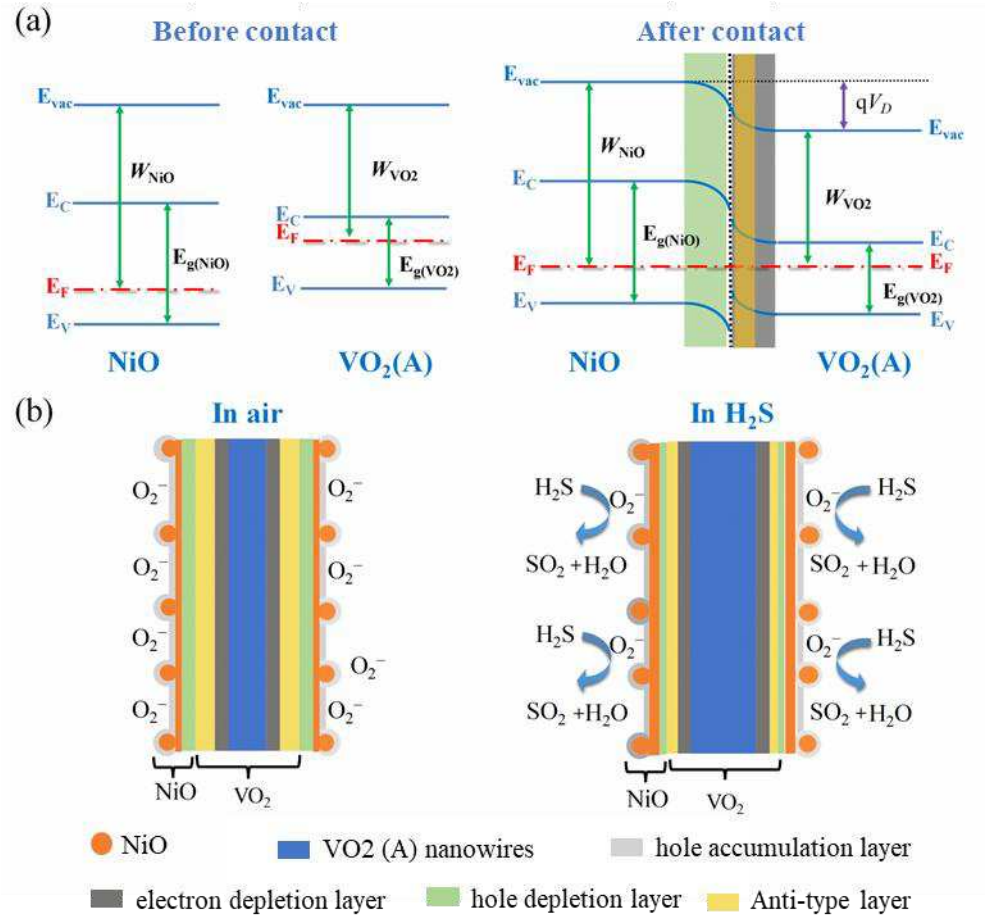


Figure 11 (a) Schematic diagram of VO_2(A)/NiO heterojunction energy band structure, (b) schematic diagram of gas sensitivity mechanism of VO_2(A)/NiO nanocomposite structure to H_2S gas

It can be seen from Fig. 11 (b) that when the VO_2(A)/NiO nanocomposite is in air, the oxygen in the air will first adsorb on the surface of the material, and then the adsorbed oxygen will capture electrons from the surface of the material to form adsorbed oxygen ions. At this point, due to the loss of electrons, a hole accumulation layer is formed on the NiO surface. And when the composite material is exposed to the H_2S atmosphere, the H_2S molecules interact with the oxygen ions chemically adsorbed on the surface of the composite sample and release electrons, and the released electrons are injected into the composite material, making the hole

accumulation layer on the NiO surface thinner, while the carrier concentration in the inversion layer on the VO_2(A) surface decreases, which will make the sensor resistance value change larger, and the corresponding sensitivity is enhanced.

The gas-sensitive response of VO_2(A)/NiO nanocomposite structure to H_2S gas is greatly enhanced by the combined effect of NiO catalytic effect and heterojunction effect. The catalytic effect of NiO on H_2S oxidation and the enhanced adsorption of H_2S molecules on the material surface due to the moderate chemical affinity between Ni and S may be the reason why the composite structure is more sensitive to H_2S gas.

In addition, in the prepared nanocomposite samples, the sample with a precursor molar ratio of 1:0.5 has the best gas-sensitive performance, which may be due to that the NiO shell layer is the thinnest and the surface nanoparticle size is the smallest in the composite samples synthesized under this condition, and some NiO ultra-thin nanosheets have also existed in the composite samples, which would greatly increase the specific surface area of the gas-sensitive materials and thus be beneficial for gas molecule adsorption. Therefore, the R-0.5 sample has the highest sensitivity to H_2S gas compared to the R-1 and R-2 samples.

4. Conclusion

One-dimensional VO_2(A)/NiO nanowires core-shell hetrojunction structure were prepared by chemical precipitation and high-temperature annealing treatment. The nanowire structure of VO_2(A) is not damaged during the annealing process. And the surface of the VO_2(A) nanowires after the composite are uniformly coated with an irregular layer of NiO nanoparticles, and the size of NiO particles gradually increases

with the increase of $Ni(NO_3)_2$ content in the precursor. The sensitivity of the gas-sensitive sensor based on this sample is up to 11.57 to 1 ppm H_2S, which is 8 times higher than that of the pure phase VO_2(A) nanowires. The enhancements of the gas-sensitive properties of the composite structure are related to the catalytic effect possessed by NiO and the formation of heterojunctions at the contact interface between VO_2(A) and NiO. VO_2(A)/NiO nanocomposites are expected to be suitable candidates for the fabrication of high-performance H_2S gas-sensitive sensors.

Author contributions

Jiran liang: Formal analysis, Funding acquisition, Project administration. Resources, Supervision, Validation, Writing-original draft. **Yinfu Zhang**: Conceptualization, Data curation, Formal analysis, Investigation, Methodology, Visualization, Writing review & editing. **Xin Wen**: Formal analysis, Investigation, Writing review. **Kangqiang Wang**: Formal analysis, Investigation, Writing review. **Haigang Liu**: Formal analysis, Investigation, Writing review. **Qian He**: Formal analysis, Investigation, Writing review. **Xiaoping Gao**: Formal analysis, Investigation, Writing review. **Wenjun Yan**: Formal analysis, Investigation, Writing review.

Declaration of competing interest

The authors declare that they have no known competing financial interests or personal relationships that could have appeared to influence the work reported in this paper.

Acknowledgements

Key R&D Plan and Transformation projects of Qinghai (2025-GX-144), the Application Research and

Development Plan of Gansu Academy of Sciences (2024YLCY-03).

Data availability

Data will be made available on request.

References

[1] A. Yu, Z. Li, J. Yi, Selective detection of parts-per-billion H_2S with Pt-decorated ZnO nanorods, Sensor Actuat B-Chem. 333 (2021) 129545. https://doi.org/10.1016/j.snb.2021.129545.

[2] A. Mirzaei, S.S. Kim, H.W. Kim, Resistance-based H_2S gas sensors using metal oxide nanostructures: A review of recent advances, J Hazard Mater. 357 (2018) 314–331. https://doi.org/10.1016/j.jhazmat.2018.06.015.

[3] A.D. Masi, P. Ascenzi, H_2S: A "Double face" molecule in health and disease, Biofactors. 39 (2013) 186–196. https://doi.org/10.1002/biof.1061.

[4] B. Yang, N.V. Myung, T. Tran, 1D Metal Oxide Semiconductor Materials for Chemiresistive Gas Sensors: A Review, Adv Electron Mater. 7 (2021) 2100271. https://doi.org/10.1002/aelm.202100271.

[5] S. Steinhauer, E. Brunet, T. Maier, G.C. Mutinati, A. Köck, Suspended CuO nanowires for ppb level H_2S sensing in dry and humid atmosphere, Sensor Actuat B-Chem. 186 (2013) 550–556. https://doi.org/10.1016/j.snb.2013.06.044.

[6] P.H. Phuoc, C.M. Hung, N. Van Toan, N. Van Duy, N.D. Hoa, N. Van Hieu, One-step fabrication of SnO_2 porous nanofiber gas sensors for sub-ppm H_2S detection, Sensor Actuat A-Phys. 303 (2020) 111722. https://doi.org/10.1016/j.sna.2019.111722.

[7] J. Liang, K. Wang, C. Xuan, Q. Chen, W. Tai, P. Ge, H. Zhang, Room temperature H_2S gas sensing performance of VO_2(A) nanowires with high aspect ratio, Sensor Actuat A-Phys. 347 (2022) 113986. https://doi.org/10.1016/j.sna.2022.113986.

[8] Z. Wang, Z. Li, T. Jiang, X. Xu, C. Wang, Ultrasensitive Hydrogen Sensor Based on Pd^0-Loaded SnO_2 Electrospun Nanofibers at Room Temperature, Acs Appl Mater Inter. 5 (2013) 2013–2021. https://doi.org/10.1021/am3028553.

[9] J. Liang, W. Wu, Q. Lou, K. Wang, C. Xuan, Room temperature NO_2 sensing performance of Ag nanoparticles modified VO_2 nanorods, J Alloy Compd. 890 (2022) 161837. https://doi.org/10.1016/j.jallcom.2021.161837.

[10] E. Espid, F. Taghipour, UV-LED Photo-activated Chemical Gas Sensors: A Review, Crit Rev Solid State. 42 (2017) 416–432. https://doi.org/10.1080/10408436.2016.1226161.

[11] Tang W., Wang J., , School of Electronic Science and Technology, Dalian University of Technology, Dalian 116023, Liaoning Province, P. R. China, Enhanced Gas Sensing Mechanisms of Metal Oxide Heterojunction Gas Sensors, Acta Phys-chim Sin. 32 (2016) 1087–1104. https://doi.org/10.3866/PKU.WHXB201602224.

[12] T.P. Mokoena, H.C. Swart, D.E. Motaung, A review on recent progress of p-type nickel oxide based gas sensors: Future perspectives, J Alloy Compd. 805 (2019) 267–294. https://doi.org/10.1016/j.jallcom.2019.06.329.

[13] M. Taeño, D. Maestre, A. Cremades, An approach to emerging optical and optoelectronic applications based on NiO micro- and nanostructures, Nanophotonics-Berlin. 10 (2021) 1785–1799. https://doi.org/10.1515/nanoph-2021-0041.

[14] M. Napari, T.N. Huq, R.L.Z. Hoye, J.L. MacManus-Driscoll, Nickel oxide thin films grown by chemical deposition techniques: Potential and challenges in next-generation rigid and flexible device applications, InfoMat. 3 (2021) 536–576. https://doi.org/10.1002/inf2.12146.

[15] L. Nie, G. Fan, A. Wang, L. Zhang, J. Guan, N. Han, Y. Chen, Finely dispersed and highly toluene sensitive NiO/$NiGa_2O_4$ heterostructures prepared from layered double hydroxides precursors, Sensor Actuat B-Chem. 345 (2021) 130412. https://doi.org/10.1016/j.snb.2021.130412.

[16] R. Li, X. Yu, X. Bian, F. Hu, Preparation and electrochemical performance of VO_2(A) hollow spheres as a cathode for aqueous zinc ion batteries, Rsc Adv. 9 (2019) 35117–35123. https://doi.org/10.1039/C9RA07340J.

[17] Partial oxidation of methane to syngas on bulk $NiAl_2O_4$ catalyst. Comparison with alumina supported nickel, platinum and rhodium catalysts, Appl Catal A-gen. 437–438 (2012) 53–62. https://doi.org/10.1016/j.apcata.2012.06.014.

[18] Y. Liu, F. Liu, J. Bai, T. Liu, Z. Yu, M. Dai, L. Zhou, H. Wang, Y. Zhang, H. Suo, G. Lu, Direct growth of NiO films on Al_2O_3 ceramics by electrochemical deposition and its excellent H_2S sensing properties, Sensor Actuat B-Chem. 296 (2019) 126619. https://doi.org/10.1016/j.snb.2019.05.096.

[19] A. Umar, H. Algadi, R. Kumar, M.S. Akhtar, A.A. Ibrahim, H. Albargi, M.A.M. Alhamami, T. Alsuwian, W. Zeng, Ultrathin Leaf-Shaped CuO Nanosheets Based Sensor Device for Enhanced Hydrogen Sulfide Gas Sensing Application, Chemosensors. 9 (2021) 221.

https://doi.org/10.3390/chemosensors9080221.

[20] S.K. Ganapathi, M. Kaur, R. Singh, V.I. Singh, A.K. Debnath, K.P. Muthe, S.C. Gadkari, Anomalous Sensing Response of NiO Nanoparticulate Films toward H_2S, Acs Appl Nano Mater. 2 (2019) 6726–6737. https://doi.org/10.1021/acsanm.9b01637.

[21] D.D. Trung, N.D. Cuong, P.L. Quang, N.T. Ngoc Anh, D.T. Quang, P.C. Nam, K.Q. Trung, S.T. Nguyen, N. Van Hieu, Facile post-synthesis and gas sensing properties of highly porous NiO microspheres, Sensor Actuat A-Phys. 296 (2019) 110–120. https://doi.org/10.1016/j.sna.2019.07.014.

[22] T. Qiu, N. Luo, M. Guo, H. Cai, Z. Cheng, J. Xu, Synthesis and Enhanced H_2S Sensing Properties of V_2O_3-NiO Nanoflower Assembled by Porous Nanosheets, J. Electrochem. Soc. 169 (2022) 037504. https://doi.org/10.1149/1945-7111/ac5653.

[23] Y. Wang, F. Qu, J. Liu, Y. Wang, J. Zhou, S. Ruan, Enhanced H_2S sensing characteristics of CuO-NiO core-shell microspheres sensors, Sensor Actuat B-Chem. 209 (2015) 515–523. https://doi.org/10.1016/j.snb.2014.12.010.

[24] J. Liang, Q. Lou, W. Wu, K. Wang, C. Xuan, NO_2 Gas Sensing Performance of a VO_2(B) Ultrathin Vertical Nanosheet Array: Experimental and DFT Investigation, Acs Appl Mater Inter. 13 (2021) 31968–31977. https://doi.org/10.1021/acsami.1c05251.

[25] D. Zhang, J. Wu, P. Li, Y. Cao, Room-temperature SO_2 gas-sensing properties based on a metal-doped MoS_2 nanoflower: an experimental and density functional theory investigation, J Mater Chem A. 5 (2017) 20666–20677. https://doi.org/10.1039/C7TA07001B.

[26] S.-C. Wang, X.-H. Wang, G.-Q. Qiao, X.-Y. Chen, X.-Z. Wang, N.-N. Wu, J. Tian, H.-Z. Cui, NiO nanoparticles-decorated ZnO hierarchical structures for isopropanol gas sensing, Rare Metals. 41 (2022) 960–971. https://doi.org/10.1007/s12598-021-01846-6.

[27] G.-J. Sun, H. Kheel, J.K. Lee, S. Choi, S. Lee, C. Lee, H_2S gas sensing properties of Fe_2O_3 nanoparticle-decorated NiO nanoplate sensors, Surface and Coatings Technology. 307 (2016) 1088–1095. https://doi.org/10.1016/j.surfcoat.2016.06.066.

[28] J. Fang, Y. Zhu, D. Wu, C. Zhang, S. Xu, D. Xiong, P. Yang, L. Wang, P.K. Chu, Gas sensing properties of NiO/SnO_2 heterojunction thin film, Sensor Actuat B-Chem. 252 (2017) 1163–1168. https://doi.org/10.1016/j.snb.2017.07.013.

[29] N. Jayababu, M Poloju, J Shruthi, MVR Reddy. NiO decorated CeO_2 nanostructures as room

temperature isopropanol gas sensors, Rsc Adv. 9 (2019) 13765-13775.

https://doi.org/10.1039/C9RA00441F